

DYNAMICS OF MAGNETIC FLUX TUBES AND THE SOLAR DYNAMO

L. H. LI¹ AND S. SOFIA

Department of Astronomy, Yale University, P.O. Box 208101, New Haven, CT 06520-8101

Draft version December 2, 2024

ABSTRACT

A magnetic flux tube is treated as a body in addition to a confined field. As a field, both the cyclonic convection (α -effect) and differential rotation (Ω -effect) play a role. As a body, the tube experiences not only a buoyant force, but also a dynamic pressure of downflows above the tube. When these two dynamic effects are incorporated into the $\alpha\Omega$ dynamo equation by adding to it two diffusion terms, we obtain the dynamic equation of a flux tube. We solve this equation by using the linear perturbation theory. The main findings are: (i) unlike the pure magnetic field, the magnetic field in the flux tube can grow up to a critical value in the convection zone when downflows are present; (ii) like the solar dynamo theory, the period is determined by the cyclonic convection and the differential rotation; (iii) the growth of the magnetic field in the flux tube is caused by both the $\alpha\Omega$ -effect and the anti-diffusion effect due to the dynamic pressure of downflows; (iv) a magnetic flux tube has an ascending phase marked by a positive growth rate, and a decay phase marked by a nonpositive growth rate; (v) two branches of the butterfly diagram occur naturally as two branches of the magnetic flux tube wave. These results are in good agreement with the relevant observations, including helioseismic observations.

Subject headings: Sun: interior — Sun: magnetic fields

1. INTRODUCTION

In contrast to the situation with the geodynamo, no breakthrough has been made in the solar dynamo problem since Parker set down the foundations for solar $\alpha\Omega$ dynamo theory in his classic 1955 paper. In this theory, differential rotation (the Ω -effect) in the solar interior shears weak poloidal magnetic fields into intense toroidal fields. Meanwhile twisting motions associated with buoyancy, turbulent convection, and the Coriolis force transform toroidal fields back into poloidal fields (the α -effect). One of the main obstacles for the $\alpha\Omega$ dynamo to operate in the convective zone, is that it requires a decreasing rotation rate outwards near the equator. This conflicts with the inferred rotation law from helioseismology (Thompson et al. 1996; Antia et al. 1998; Schou et al. 1998; Antia & Basu 2000). The second main obstacle, is that most of the magnetic flux in the solar photosphere, and presumably below, is present in a strongly intermittent form, being concentrated into strong flux tubes. Due to buoyancy instabilities, these structures cannot be stored in the convective zone for a timescale comparable to the cycle period. Without any force to balance the buoyancy, the instabilities can rapidly remove the whole tube from the zone (Parker 1975).

It is possible that something important has been missed in the dynamo theory. Since most of the magnetic flux is present in strong flux tubes, we should consider the magnetic field as an entity that experiences self-diffusion, and dynamic pressure of the flow. Also, since stratification provides a preferred direction, turbulence in the convective zone of the Sun is anisotropic. Numerical simulations of the solar outer convection zone (Chan and Sofia 1989; Kim & Chan 1998; Nordlund 1999), indicate a major presence of downward-moving plumes. This suggests that the dynamic pressure of the downward-moving flow may

push down the magnetic flux tubes to prevent them from rising, until they reach certain depth in the convective zone.

In fact, helioseismic inversions made by Antia, Chitre, and Thompson (2000) indicate that there is a magnetic field of approximately 20 kG strength located at a depth of $r = 0.96 R_\odot$ in 1996, and Li & Sofia (2001) find that this magnetic field can produce the observed cyclic variations of total solar irradiance (Fröhlich & Lean 1998), solar effective temperature (Gray & Livingston 1997), and solar radius (Emilio et al 2000). These suggest that the magnetic field can be stored within the convective zone, for a timescale comparable to the cycle period, when the downflows are present. In this paper, we propose an $\alpha\Omega$ dynamo model which includes these key points, and obtain a solar dynamo model which explains both the low and high altitude branches of the butterfly diagram (Makarov & Sivaraman 1989), without facing the buoyancy stability problem.

2. BASIC EQUATIONS

We consider a magnetic flux tube with radius a and length L . Its magnetic field \mathbf{B} is assumed to be uniform. As usual, we decompose it into a toroidal and a poloidal component,

$$\mathbf{B} = B\mathbf{e}_\phi + \nabla \times (A\mathbf{e}_\phi). \quad (1)$$

The local hydrostatic equilibrium of the flux tube in the solar interior requires

$$P = P_i + B^2/8\pi, \quad (2)$$

where P and P_i are the total and internal gas pressure, respectively. Assuming that this equilibrium in the flux tube is reached solely by adjusting its density, then the internal density ρ_i is related to the normal density ρ by

$$\rho_i = \rho P_i/P. \quad (3)$$

¹also at Purple Mountain Observatory, Chinese Academy of Sciences, and National Astronomical Observatories, Chinese Academy of Sciences, 2 Beijing Road West, Nanjing, Jiangsu 210008, China

As a result, the density reduction of the magnetic flux tube is

$$\rho - \rho_i = \rho B^2 / 8\pi P. \quad (4)$$

The reduced density inside the flux tube produces a buoyant force,

$$\mathbf{F} = \pi a^2 L g (\rho - \rho_i) \mathbf{e}_r, \quad (5)$$

where g is the gravitational acceleration. We assume that a is smaller than the pressure scale height so that we can consider that the gas density of the flux tube is uniform. In this case, the total mass contained in the flux tube equals

$$M_i = \pi a^2 L \rho (1 - B^2 / 8\pi P). \quad (6)$$

Therefore, the buoyant acceleration g_b can be expressed by the gravitational acceleration g , total pressure P and the magnetic field B as follows:

$$g_b = g B^2 / (8\pi P - B^2). \quad (7)$$

If there is no downward flow to balance this pressure, the only force that goes against the buoyant force is the aerodynamic drag,

$$\mathbf{F}_d = -\frac{1}{2} C_d \rho u^2 a L \mathbf{e}_r, \quad (8)$$

where u is the velocity of rise and $C_d (\sim 1)$ is the drag coefficient. Taking into account both the buoyant force and the drag force, as done by Parker (1975), the terminal velocity of rise occurs for $F = F_d$, yielding the rate of rise

$$u = \left(\frac{2\pi a g \rho - \rho_i}{C_d \rho} \right)^{1/2} = V_A \left(\frac{\pi a}{C_D H_p} \right)^{1/2}, \quad (9)$$

where $H_p = P/\rho g$ is the pressure scale height, $V_A = B/(4\pi\rho)^{1/2}$ is the Alfvén speed. The rise time to the surface is smaller than the required field amplification time of about 10 years by the classical dynamo theory, as estimated by Parker (1975).

However, numerical simulations of the Sun's outer convection zone made, e.g. by Nordlund (1999), indicate a major presence of downward-moving plumes of high velocity. This downward flow has an inward dynamic pressure ρv_z^2 . If this pressure can balance the buoyant force of the flux tube, then the flux tube can be stored in the convection zone so that it can be amplified by the $\alpha\Omega$ dynamo. Antia et al (2000) employ the observed splittings of solar oscillation frequencies to separate the effects of interior solar rotation, and to estimate the contribution from a large-scale magnetic field. After subtracting out the estimated contribution from rotation, there is some residual signal in the even splitting coefficients. This may be explained by a magnetic field of approximately 20 kG strength located at $r = 0.96 R_\odot$ in 1996. Since the density here is of order 4×10^{-3} , and the downward velocity for the plumes is of order $5 \times 10^4 \text{ cm s}^{-1}$ (Nordlund 1999), the estimated dynamical pressure of the plumes, ρv^2 , is equal to or larger than $10^7 \text{ dyne cm}^{-2}$. The size of ρv^2 is comparable with the magnetic pressure, $B^2/8\pi$, for a field strength of 20 – 30 kG. Therefore, as a body, a magnetic flux tube experiences not only a buoyant force, but also a dynamic pressure of downflows. The total pushdown force of downward plumes equals to the dynamic pressure (ρv_z^2) times the total cross section of the plumes (S). The dynamic acceleration g_n can be expressed as follows:

$$g_n = 2s v_z^2 \xi / \pi a, \quad (10)$$

where $s = 1$ when $v_z > 0$, $s = -1$ when $v_z < 0$, $\xi = S/2aL \leq 1$ is the fractional area of the downflows. The upward-moving plumes underneath the flux tube ($s = 1$) accelerate the magnetic buoyant diffusion of the tube, while the downward-moving plumes above the flux tube ($s = -1$) go against the magnetic diffusion. These downflows act as an anti-diffusion process.

As a magnetic field, the field in a flux tube must obey the hydromagnetic induction equation (Parker 1955),

$$\frac{\partial \mathbf{B}}{\partial t} = \nabla \times (\mathbf{U} \times \mathbf{B} + \vec{\mathcal{E}}) - \nabla \times (\eta \nabla \times \mathbf{B}). \quad (11)$$

We assume a pure rotation motion $\mathbf{U} = \boldsymbol{\Omega} \times \mathbf{r}$, where $\boldsymbol{\Omega}$ is the angular velocity. This will cause the Ω -effect. $\vec{\mathcal{E}}$ contains the α -effect, $\alpha\mathbf{B}$, and the magnetic diffusion processes, which are caused by the turbulent pressure, $\beta_t \nabla \times \mathbf{B}$, by the magnetic buoyant force, $\beta_b \nabla \times \mathbf{B}$, and by the dynamic pressure of downward-moving plumes, $\beta_n \nabla \times \mathbf{B}$. Therefore,

$$\vec{\mathcal{E}} = \alpha \mathbf{B} - (\beta_t + \beta_b + \beta_n) \nabla \times \mathbf{B}. \quad (12)$$

The magnetic diffusion caused by the microscopic gas collision motion, has been included in Eq. (11) in terms of the classic magnetic diffusivity, $\eta \nabla \times \mathbf{B}$. For convection, α can be approximately expressed as (Hrause & Rädler 1980)

$$\alpha = \frac{1}{3} h \tau_{\text{cor}}, \quad (13)$$

where $h = \overline{\mathbf{v} \cdot (\nabla \times \mathbf{v})}$ is the mean helicity over the correlation time τ_{cor} .

In order to work out the various magnetic diffusivities mentioned above, we observe that the diffusivity of a force is proportional to its impulse per unit mass. The impulse is defined as the force times its action time. The impulse per unit mass has the dimension of acceleration times time. The action time can be taken to be the propagation time of magnetic perturbation across the diameter of the flux tube. Since the characteristic propagation velocity of magnetic perturbations is the Alfvén velocity V_A , the action time is estimated to be $t_{\text{act}} = 2a/V_A$. However, diffusivity has the dimension of acceleration times time times length. The characteristic length for a flux tube is its length L . We use this length L to meet the need of dimensionality for the buoyant and the dynamic diffusivity. Consequently, we have

$$\beta_b = g_b (2a/V_A) L = (4\pi\rho)^{1/2} 2a g L B / (8\pi P - B^2), \quad (14)$$

$$\beta_n = g_n (2a/V_A) L = (4\pi\rho)^{1/2} 4s v_z^2 \xi L / \pi B. \quad (15)$$

The magnetic turbulent diffusivity $\beta_t = \frac{1}{3} v'^2 \tau_{\text{cor}}$ is known (Hrause & Rädler 1980) for an isotropic turbulence, where v' is the turbulent velocity.

In summary, we define

$$\beta = \eta + \beta_t + \beta_b + \beta_n, \quad (16)$$

where β_b and β_d are given by (14) and (15), respectively. As a result, the hydromagnetic induction equation becomes the dynamic equation of a magnetic flux tube,

$$\frac{\partial \mathbf{B}}{\partial t} = \nabla \times (\mathbf{U} \times \mathbf{B} + \alpha \mathbf{B}) - \nabla \times (\beta \nabla \times \mathbf{B}). \quad (17)$$

Since β depends on \mathbf{B} , this equation is nonlinear.

3. LINEAR ANALYSIS

3.1. Linearization equations

Substituting Eq. (1) into Eq. (17), and linearizing the result with respect to the perturbation of B and A near B_0 and $A_0 = 0$, denoted by B' and A' , we obtain two linear equations that govern B' and A' ,

$$\frac{\partial A'}{\partial t} = \alpha B' + \beta_0 \nabla^2 A', \quad (18)$$

$$\begin{aligned} \frac{\partial B'}{\partial t} &= \hat{\Omega}_z \frac{\partial A'}{\partial x} - \hat{\Omega}_x \frac{\partial A'}{\partial z} - \alpha \nabla^2 A' + \beta_0 \nabla^2 B' \\ &\quad + \hat{\beta}_B B' - \hat{\beta}_z \frac{\partial B'}{\partial z} + \hat{\beta}_x \frac{\partial B'}{\partial x} \end{aligned} \quad (19)$$

in the local Cartesian frame $\mathbf{e}_z = \mathbf{e}_r$, $\mathbf{e}_y = \mathbf{e}_\phi$, $\mathbf{e}_x = \mathbf{e}_\theta$. We have defined,

$$\hat{\Omega}_x = \frac{\partial}{\partial x}(r\Omega \sin \theta) = \Omega(\cos \theta + \hat{\Omega}_\theta \sin \theta), \quad (20)$$

$$\hat{\Omega}_z = \frac{\partial}{\partial z}(r\Omega \sin \theta) = \Omega \sin \theta(1 + \hat{\Omega}_r), \quad (21)$$

$$\hat{\beta}_B = \hat{\beta} \nabla^2 B_0 - \frac{\partial \hat{\beta}}{\partial z} \frac{\partial B_0}{\partial z} + \frac{\partial \hat{\beta}}{\partial x} \frac{\partial B_0}{\partial x}, \quad (22)$$

$$\hat{\beta}_x = \frac{\partial \beta_0}{\partial x} + \hat{\beta} \frac{\partial B_0}{\partial x}, \quad (23)$$

$$\hat{\beta}_z = \frac{\partial \beta_0}{\partial z} + \hat{\beta} \frac{\partial B_0}{\partial z}, \quad (24)$$

where $\beta_0 = \beta(B_0, v_z)$, $\hat{\Omega}_\theta = \partial \ln \Omega / \partial \theta$, $\hat{\Omega}_r = \partial \ln \Omega / \partial \ln r$, and $\hat{\beta} = (\partial \beta / \partial B)|_{B=B_0} = [\beta_1(B_0) - \beta_2(B_0, v_z)]/B_0$. The second line of Eq. (19) stands for the nonuniform effect. When this effect is ignored, Eqs. (18-19) are the same as the classic dynamo equations, except that β_0 depends on the magnetic field and the convection velocity field v_z . In the classic case, β_0 is always positive, implying a genuine diffusion. In contrast, when the dynamic pressure of the downward moving plumes is larger than the buoyant pressure of the flux tube, β_0 can become negative.

3.2. Dispersion relation

In order to investigate the linear instability, we try the wavelike solutions of the form

$$B' = B'_0 \exp[i(\omega t - \mathbf{k} \cdot \mathbf{x})], \quad (25)$$

$$A' = A'_0 \exp[i(\omega t - \mathbf{k} \cdot \mathbf{x})], \quad (26)$$

where ω is complex, while the other variables are real. Substituting Eqs. (25-26) into Eqs. (18-19), we obtain

$$(\beta_0 k^2 + i\omega) A'_0 = \alpha B'_0, \quad (27)$$

$$(\beta_0 k^2 + i\omega - \hat{\beta}_B + i\hat{\beta}_k) B'_0 = -i(k_x \hat{\Omega}_z - k_z \hat{\Omega}_x) A'_0, \quad (28)$$

where $\hat{\beta}_k = \hat{\beta}_x k_x - \hat{\beta}_z k_z$. The dispersion equation can be obtained by multiplying Eq. (27) and (28),

$$(\beta_0 k^2 + i\omega)(\beta_0 k^2 + i\omega - \hat{\beta}_B + i\hat{\beta}_k) = -i\alpha(k_x \hat{\Omega}_z - k_z \hat{\Omega}_x). \quad (29)$$

Solving this equation for ω as a function of wavenumber vector \mathbf{k} , we obtain the dispersion relation,

$$\omega = \omega(k_x, k_y, k_z; v_z, B_0), \quad (30)$$

where B_0 and v_z are parameters.

Under the homogeneity approximation, we can neglect $\hat{\beta}_B$ and $\hat{\beta}_k$. In this case, Eq. (29) reduces to

$$(\beta_0 k^2 + i\omega)^2 = -i\alpha(k_x \hat{\Omega}_z - k_z \hat{\Omega}_x). \quad (31)$$

Rewriting $-i$ as $\exp(i3\pi/2)$, when

$$D = \alpha(k_x \hat{\Omega}_z - k_z \hat{\Omega}_x)/2 \geq 0 \quad (32)$$

is satisfied, we can solve this equation for ω easily as follows:

$$\omega_\pm = \pm \sqrt{D} + i(\beta k^2 \mp \sqrt{D}). \quad (33)$$

3.3. Period

When $D \neq 0$, the magnetic flux tube generation is periodic. The period is

$$T = 2\pi/\sqrt{D}. \quad (34)$$

It is well-known that α is positive (negative) for cyclonic convection in the northern (southern) hemisphere of the Sun. Therefore, the condition $D > 0$ leads to

$$(1 + \hat{\Omega}_r)k_x > (\cot \theta + \hat{\Omega}_\theta)k_z, \quad (35)$$

where \cot is the cotangent triangle function. When this condition is satisfied we have two magnetic flux tube waves propagating in the opposite direction. These two waves have the same period.

In order to calculate T , we first determine k_x and k_z . The fundamental wavenumber is, $k_{x0} = \sqrt{2}\pi/r$ in the x -axis, and $k_{z0} = 2\pi/r$ in the z -axis at r since the maximum wavelengths are $\lambda_{x0} = \sqrt{2}r$ and $\lambda_{z0} = r$. The butterfly diagram implies that both branches share the whole length, so we assume $k_x^\pm = \pm k_{x0}$ for the equatorward/poleward branch in the northern hemisphere of the Sun. The condition $D > 0$ leads to $k_z^\pm = \pm k_{z0}$ in the same hemisphere.

Helioseismic data allow us to probe the rotation rate in the solar interior as a function of radius and latitude (Thompson et al. 1996; Antia et al. 1998; Schou et al. 1998; Antia & Basu 2000). We use the rotation rate inferred from Global Oscillation Network Group (GONG) data by Antia, Basu, and Chitre (1998), as shown in Fig. 1.

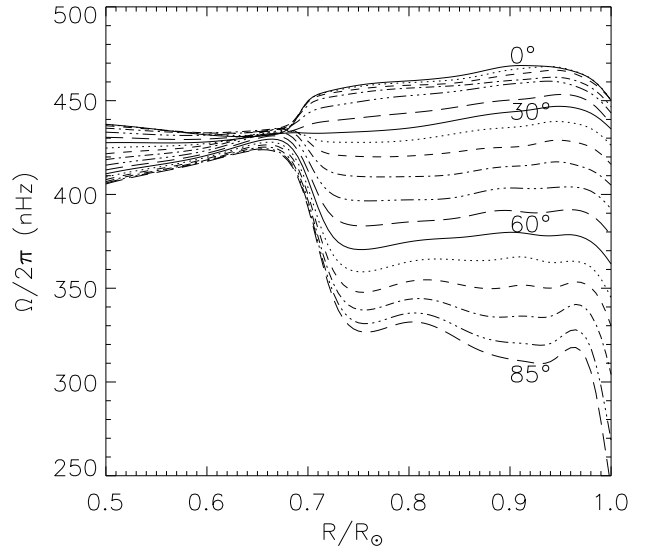


FIG. 1.— Solar rotation rate as a function of radius and latitude (Antia et al. 1998).

Table 1 shows T (unit: year) as a function of radius and latitude, calculated by using Eq. (34). This table predicts

a low latitude branch and a high latitude branch. Since the observed length of the solar cycles is equal to about 22 years, this table shows that the cycle should originate from the surface layer with $r > 0.95R_\odot$, which is in agreement with the inferred depth from helioseismic data by Antia, Chitre and Thompson (2000), who found that the solar magnetic field peaks at $r = 0.96R_\odot$. The period also depends on latitude. If we use the observed period (22 years) as a criterion, this table shows that the low- (high-) latitude branch originates from the latitude 35° (40°). Since $k_x > 0$ and $k_z > 0$ for the low-latitude branch, the magnetic flux tubes near the latitude 35° and radius $r = 0.96R_\odot$ move upwards and equatorwards. Since $k_x < 0$ and $k_z < 0$ for the high-latitude branch, the the magnetic flux tubes near 40° and $0.96R_\odot$ move downwards and polewards. This scenario is in agreement with observations (Makarov & Sivaraman 1989).

For different branches we have to use different α values to produce the desired period at the mid latitude. Since α is determined by the Coriolis force and the higher the Coriolis force the lower the latitude, it is reasonable to use a larger α for the low-latitude branch. Nevertheless, a jump of α from 90 cm s^{-1} at 35° to 5 cm s^{-1} at 40° is implied and needs to be explained.

Table 1 also shows that solar magnetic activity is a multi-period phenomenon, and the longest period is 22 years, occuring in the latitude range from 35° to 40° . The period decreases equatorwards, polewards, and downwards. The period can be as small as 1-2 year near the base of the convection zone and near the equator.

3.4. Critical magnetic field

Eqs. (25-26) show that spontaneous generation of a magnetic flux tube requires $\omega_I = (\beta k^2 \mp \sqrt{D}) < 0$, which implies

$$\beta < \pm \sqrt{D}/k^2. \quad (36)$$

For simplicity, we further neglect the classic collision and isotropic turbulent diffusivity. As a result, the unstable condition (36) becomes

$$\beta_b + \beta_n \mp \sqrt{D}/k^2 < 0. \quad (37)$$

We assume $B_0 \ll B_g$, where $B_g = (8\pi P)^{1/2}$ is the magnetic field strength when the magnetic pressure equals to the total pressure P . In this case inequality (37) is quadratic since $\beta_b \approx (4\pi\rho)^{1/2} 2agLB/B_g^2$. Solving this quadratic inequality for B_0 , we obtain

$$B_-^+ < B_0 < B_+^+ \quad (38)$$

for the ω_+ branch, where

$$B_\pm^+ = B_g \left[\left(\frac{DP}{8\rho a^2 L^2 g^2 k^4} \right)^{1/2} \pm \left(\frac{DP}{8\rho a^2 L^2 g^2 k^4} - \frac{2s\xi v_z^2}{\pi ag} \right)^{1/2} \right] \quad (39)$$

is the critical magnetic field for the ω_+ branch. When B_\pm^+ is complex, we set $B_\pm^+ = 0$. For this branch, we have both upper and lower critical magnetic field. The former is non-negative, while the latter can be negative. The fact that B_0 represents the amplitude of the toroidal field requires

$$B_0 > 0. \quad (40)$$

Therefore, when $B_-^+ < 0$ we reset $B_-^+ = 0$. When $B_+^+ = B_-^+ = 0$, this branch vanishes. When $v_z < 0$, $s = -1$. In this case $B_-^+ < 0$. So we reset it to be zero.

Similarly, solving inequality (37) for B_0 , we obtain

$$B_-^- < B_0 < B_+^-, \quad (41)$$

for the ω_- branch, where

$$B_\pm^- = B_g \left[- \left(\frac{DP}{8\rho a^2 L^2 g^2 k^4} \right)^{1/2} \pm \left(\frac{DP}{8\rho a^2 L^2 g^2 k^4} - \frac{2s\xi v_z^2}{\pi ag} \right)^{1/2} \right]. \quad (42)$$

When B_\pm^- is complex, we set $B_\pm^- = 0$. For this branch, we also have both upper and lower critical magnetic field. However, the latter is always non-positive, so we reset $B_-^- = 0$. The former can be negative, too. When $B_+^- < 0$ we reset $B_+^- = 0$. When $B_+^- = B_-^- = 0$ this branch vanishes since $B_0 > 0$ is required. Only when $v_z < 0$ is B_+^- positive.

From Eqs. (39) and (42) we can see that the critical magnetic field of a magnetic flux tube depends on not only the velocity (including direction s and speed $|v_z|$) of flows, the size (including radius a and length L) of the flux tube, and its location, but also the fractional area ξ . When the $\alpha\Omega$ -effect is neglected (letting $D = 0$), the critical field is determined by competition between buoyant force and dynamic pressure of downflows,

$$B_+^\pm = B_g (-2s\xi v_z^2 / \pi ag)^{1/2}. \quad (43)$$

This is equivalent to the magnetic field by equating the buoyant and dynamic acceleration given in Eq. (7) and Eq. (10). Obviously, the critical field does not vanish only when there is a downflow so that $s = -1$ and $\xi \neq 0$. In fact, sunspots are often observed near the edges of granulations where there exist downflows. The critical field is proportional to the speed of downflows, but inversely proportional to the square root of the radius of the flux tube. Table 2 shows B_+^\pm (unit: gauss) as a function of solar radius and latitude with $a = 2000 \text{ km}$, $v_z = -0.5 \text{ km s}^{-1}$, $\xi = 1$, and $L = 10a$. The other parameters are the same as in Table 1. This table shows that the shallower the solar layer, the weaker the critical field, as expected.

When the $\alpha\Omega$ -effect is included in, the critical magnetic field for the equatorward branch is not zero even if there is no downflow. In this case, Eq. (39) reduces to

$$B_+^+ = B_g \left(\frac{DP}{2\rho a^2 L^2 g^2 k^4} \right)^{1/2}. \quad (44)$$

Obviously, the thinner and shorter the flux tube the larger the critical magnetic field. Table 3 shows this critical field as a function of solar radius and latitude, using the same parameters as in Table 2. In this case, the critical field for another branch is zero. Comparing Table 3 with Table 2, we can see that the critical field without downflows is weaker than the corresponding field with downflows. Nevertheless, it does not vanish. The reason is that $\alpha\Omega$ -effect goes against the buoyant instability.

3.5. Growth rate

From the dispersion relation given by Eq. (33), we find the growth rate for the ω_{\pm} branch,

$$\begin{aligned}\Gamma^{\pm} &= -\omega_I^{\pm} = -(\beta_b + \beta_n)k^2 \pm \sqrt{D} \\ &= \frac{\sqrt{2}agLk^2}{c} \frac{(B_+^{\pm} - B_0)(B_0 - B_-^{\pm})}{B_g|B_0|},\end{aligned}\quad (45)$$

where $c = (P/\rho)^{1/2}$ is the sound speed, and B_{\pm}^{\pm} are given in Eqs. (39) and (42). Obviously, the growth rate is positive when

$$B_-^{\pm} < B_0 < B_+^{\pm}, \quad (46)$$

zero when $B_0 = B_{\pm}^{\pm}$, negative otherwise. This predicts that a magnetic flux tube experiences an ascending phase and a descending phase, implying that sunspots grow slowly, last for some time, and then disappear, since a sunspot appears when a flux tube crosses the surface of the Sun. This is in good agreement with sunspot observations.

Eq. (45) shows two wave branches, one that propagates equatorwards, and another that propagates polewards, can be excited when $v_z < 0$. Table 4 shows the required time τ^{\pm}

$$\tau^{\pm} = \int_{B_1}^{B_+^{\pm}} [B\Gamma^{\pm}(B)]^{-1} dB \quad (47)$$

for the tube field growth from $B_1 = 10^{-3}B_+^{\pm}$ to B_+^{\pm} as a function of solar radius and latitude, in which $L = 10a$ and the other parameters are the same as in Table 2.

When $v_z = 0$, Eq. (45) reduces to

$$\Gamma^{\pm} = \pm\sqrt{D} - \beta_b k^2. \quad (48)$$

This shows the magnetic field in a magnetic flux tube can grow since the $\alpha\Omega$ -effect can go against the buoyant instability in the equatorward branch even if there is no downflow. Nevertheless, the growth rate is much smaller than that with downflows, as shown in Table 5, in which the same parameters are used as in Table 4, except that $v_z = 0$.

3.6. Magnetic flux tube waves

Solving Eq. (27) for A'_0 , we can express the temporal evolution of the toroidal magnetic field B and the poloidal vector potential A in terms of the initial field B_0 for each magnetic flux tube as follows:

$$B^{\pm} = B_0 e^{\Gamma^{\pm}t} \exp \left[i \left(\frac{2\pi t}{T} \mp \mathbf{k} \cdot \mathbf{x} \right) \right], \quad (49)$$

$$A^{\pm} = B_0 \frac{\alpha T}{4\pi} e^{\Gamma^{\pm}t} \exp \left[i \left(\frac{2\pi t}{T} \mp \mathbf{k} \cdot \mathbf{x} - \frac{\pi}{4} \right) \right]. \quad (50)$$

The wavenumber vector \mathbf{k} should satisfy Eq. (32). Substituting Eqs. (49-50) into Eq. (1), we obtain,

$$\begin{aligned}\mathbf{B}^{\pm} &= B_0 e^{\Gamma^{\pm}t} \exp \left[i \left(\frac{2\pi t}{T} \mp \mathbf{k} \cdot \mathbf{x} + \phi^{\pm} \right) \right] \cdot \{\mathbf{e}_{\phi} \\ &+ \frac{\alpha T}{4\pi} (-k_z \mathbf{e}_x + k_x \mathbf{e}_z) \exp \left[-i \frac{\pi}{4}(1 \pm 2) \right]\},\end{aligned}\quad (51)$$

where $k_x = \sqrt{2}\pi/r$, $k_z = 2\pi/r$ and $k_y = 0$ are required by the condition $D > 0$, and ϕ^{\pm} are the initial phase angles for these two branches.

This equation shows that the toroidal field leads the poloidal field by a phase of $3\pi/4$ for the equatorward branch, but lags the poloidal field by a phase of $\pi/4$ for the poleward branch. The former is in agreement with the observations, which reveal that the poloidal component is almost in antiphase with the toroidal component. Table 6 shows the ratio of the poloidal to toroidal component, in percentages. Obviously, the poloidal component is weaker than the toroidal component, which is in agreement with observations.

From Table 4 it can be seen that the required time for the magnetic field of a typical magnetic flux tube to grow from a very low level to the critical field is very short in comparison with the cycle period when downflows are present. Using Eq. (47) it is easy to check that the decay time for such a magnetic flux tube is of the same order of magnitude as the growth time. Observations show that sunspots last, on average, a week or two. Therefore, our theory and observations are in agreement with each other. However, this timescale is much shorter than the cycle period. This suggests that magnetic flux tubes are only the basic elements of the magnetic flux tube wave described by Eq. (17). Therefore, we use the total magnetic flux $\Phi = N\pi\bar{a}^2\mathcal{B}$ rather than the magnetic field strength B for each magnetic flux tube as the wave variable of the magnetic flux tube wave, where N is the total number of magnetic flux tubes present at the same time, \bar{a} is the statistically averaged radius of magnetic flux tubes, and \mathcal{B} is the statistically averaged magnetic field strength of magnetic flux tubes. Since \bar{a} and \mathcal{B} are mean quantities, only the number of flux tubes is variable, we finally find that the flux tube number varies with time and latitude

$$N = N_0 \exp \left[i \left(\frac{2\pi t}{T} \mp \mathbf{k} \cdot \mathbf{x} + \phi^{\pm} \right) \right], \quad (52)$$

since $x = r[1 + \tan(\pi/4 - \theta)]/\sqrt{2}$, where θ is the latitude. N_0 is a constant in our single-tube theory.

By fixing $z = R_{\odot}$ and setting

$$2\pi t/T \mp k_x x + \phi^{\pm} = (n - 1)\pi, \quad (53)$$

where $n = 1, 2, 3, \dots$ is an integer, we can investigate how the wave peak propagates with time. Since $k_x = \sqrt{2}\pi/r$, we obtain the migration equations for both branches

$$\theta^+ = \frac{\pi}{4} - \tan^{-1} \left[\frac{t}{T} - \frac{n-1}{2} + \tan \left(\frac{\pi}{4} - \frac{35\pi}{180} \right) \right], \quad (54)$$

$$\theta^- = \frac{\pi}{4} + \tan^{-1} \left[\frac{t}{T} - \frac{n-1}{2} + \tan \left(\frac{\pi}{4} - \frac{50\pi}{180} \right) \right], \quad (55)$$

where we have assumed $\phi^+ = 35^\circ$, and $\phi^- = 50^\circ$, as revealed by observations (Makarov & Sivaraman 1989). Obviously, the integer n plays a role of cycle number if we increase it by 1 when t/T increases by 1/2. These two equations are the mathematical expressions for the butterfly diagram.

Since N_0 is a constant in our single-tube theory, we predict that the total number of flux tubes, on average, does not vary with time. This is in conflict with observations, which show that the sunspot number increases in the ascending phase, and then decrease in the descending phase of the solar cycle. This problem may be solved by taking into account interactions between magnetic flux tubes.

4. CONCLUSION

Most of the magnetic flux in the solar photosphere, and presumably below, is present in the form of strong magnetic flux tubes. The classical dynamo theory focuses on amplification of the magnetic field itself, and it fails to reproduce the main features of the activity cycle. We develop here a dynamo theory which considers the field as made up of flux tubes, and includes the dynamic behavior of those tubes, which we treat as discrete bodies. As a field, both the cyclonic convection (α -effect) and differential rotation (Ω -effect) play a role. As a body, the tube experiences not only a buoyant force, but also a dynamic pressure of downflows above the tube. When these two dynamic effects are incorporated into the $\alpha\Omega$ dynamo equation by adding to it two diffusion terms, we obtain the dynamic equation of a flux tube. Solving these equations using the linear perturbation theory, we find the cycle length, the growth rate, and the critical magnetic field. The main findings are:

- Unlike the pure magnetic field, the magnetic field in flux tubes can grow up to a critical value in the convection zone when downflows are present;
- Like the solar dynamo theory, the period is

determined by the cyclonic convection and the differential rotation;

- Amplification of the magnetic field in the flux tube is caused by both the $\alpha\Omega$ -effect and the anti-diffusion effect due to the dynamic pressure of downflows;
- A magnetic flux tube has an ascending phase marked by a positive growth rate, and a decay phase marked by a nonpositive growth rate;
- Two branches of the butterfly diagram occur naturally as two branches of the magnetic flux tube wave.

These results are in good agreement with the relevant observations, including helioseismic observations.

We want to thank Dr. Sarbani Basu for her kindly providing us with rotation rate data, Dr. Frank J. Robinson for his help, and Prof. Pierre Demarque for useful discussions. This work was supported in part by a grant from the National Aeronautics and Space Administration, and in part by Natural Science Foundation of China (project 19675064).

REFERENCES

Antia, H. M., Basu, S., & Chitre, S. M. 1998, *Mon. Not. Roy. Astron. Soc.* 298, 543
 Antia, H.M., Chitre, S.M., & Thompson, M.J. 2000, *A&A*, 360, 335
 Antia, H.M., & Basu, S. 2000, *ApJ*, 541, 442
 Belvedere, G. 1985, *Sol. Phys.*, 100, 363
 Chan, K.L. & Sofia, S. 1989, *ApJ*, 336, 1022
 Emilio, M., Kuhn, J.R., Bush, R.I. & Scherrer, P. 2000, *ApJ*, 543, 1007.
 Fröhlich, C. & Lean, J. 1998, in IAU Sympsiium 185: New Eyes to See Inside the Sun and Stars, ed. F.L. Deubner, (Dordrecht: Kluwer Academic Publ.), 89
 Gray, D.F. & Livingston, W.C. 1997, *ApJ*, 474, 802
 Kim, Y-C & Chan, K.L. 1998, *ApJ*, 496, L121
 Krause, F. & Rädler, K. H. 1980, *Mean-field Magnetohydrodynamics and Dynamo theory* (Pergamon: Oxford)
 Li, I. H., & Sofia, S. 2001, *ApJ*, 249, 1204
 Makarov, V. I., & Sivaraman, K. R. 1989, *Sol. Phys.*, 123, 367
 Nordlund, Å 1999, IAU Colloquium 179 on Cyclical evolution of solar magnetic fields: Advances in theory and observations.
 Parker, E. N. 1955, *ApJ*, 122, 293
 Parker, E. N. 1975, *ApJ*, 198, 205
 Schou, J. et al. 1998, *ApJ*, 505, 390
 Thompson, M. J., et al. 1996, *Science*, 272, 1300

TABLE 1
THE LENGTH OF SOLAR CYCLE (UNIT: YEAR) AS A FUNCTION OF RADIUS AND LATITUDE.

R	$k_x = \frac{\sqrt{2}\pi}{r}$, $k_z = \frac{2\pi}{r}$, $\alpha = 90 \text{ cm s}^{-1}$									$k_x = -\frac{\sqrt{2}\pi}{r}$, $k_z = -\frac{2\pi}{r}$, $\alpha = 5 \text{ cm s}^{-1}$								
	0°	5°	10°	15°	20°	25°	30°	35°	40°	45°	50°	55°	60°	65°	70°	75°	80°	85°
0.72	1	1	2	2	3	4	19	19	13	10	8	7	6	5	4	3	2	
0.73	1	1	2	2	3	4	19	19	13	10	8	7	6	5	4	3	2	
0.74	1	1	2	2	3	4	20	19	13	10	8	7	6	5	4	3	2	
0.75	1	2	2	2	3	4	20	19	13	10	8	7	6	5	4	3	2	
0.76	1	2	2	2	3	4	19	19	13	10	8	7	6	5	4	3	2	
0.77	1	2	2	2	3	4	19	19	13	10	8	7	6	5	4	3	2	
0.78	1	2	2	2	3	4	20	20	13	10	8	7	6	5	4	3	2	
0.79	1	2	2	2	3	4	20	20	13	10	9	7	6	5	4	3	2	
0.80	1	2	2	2	3	4	20	20	13	10	9	7	6	5	4	3	2	
0.81	1	2	2	2	3	4	20	20	13	10	9	7	6	5	4	3	2	
0.82	1	2	2	2	3	4	20	20	13	11	9	7	6	5	4	3	2	
0.83	1	2	2	2	3	4	20	20	14	11	9	7	6	5	4	3	2	
0.84	1	2	2	2	3	4	20	20	14	11	9	7	6	5	4	3	2	
0.85	1	2	2	2	3	4	20	20	14	11	9	7	6	5	4	3	2	
0.86	1	2	2	2	3	4	20	20	14	11	9	7	6	5	4	3	2	
0.87	2	2	2	2	3	4	21	21	14	11	9	8	6	5	4	3	2	
0.88	2	2	2	2	3	4	21	21	14	11	9	8	6	5	4	3	2	
0.89	2	2	2	2	3	4	21	21	14	11	9	8	6	5	5	3	2	
0.90	2	2	2	2	3	4	21	21	14	11	9	8	7	6	5	4	2	
0.91	2	2	2	2	3	4	21	21	14	11	9	8	7	6	5	4	2	
0.92	2	2	2	2	3	4	21	21	14	11	9	8	7	6	5	4	2	
0.93	2	2	2	2	3	4	21	21	14	11	9	8	7	6	5	4	2	
0.94	2	2	2	2	3	4	21	21	14	11	9	8	7	6	5	4	2	
0.95	2	2	2	2	3	4	21	21	14	11	9	8	7	6	5	4	2	
0.96	2	2	2	2	3	5	22	22	15	11	9	8	7	6	5	4	2	
0.97	2	2	2	2	3	5	22	22	15	11	9	8	7	6	5	4	2	
0.98	2	2	2	2	3	5	22	22	15	12	10	8	7	6	5	4	2	
0.99	2	2	2	2	3	5	22	22	15	12	10	8	7	6	5	4	3	
1.00	2	2	2	2	3	5	22	22	15	12	10	8	7	6	5	4	3	

TABLE 2

CRITICAL MAGNETIC FIELD (GAUSS) AS A FUNCTION OF RADIUS AND LATITUDE WITH DOWNFLOWS.

TABLE 3

CRITICAL MAGNETIC FIELD (GAUSS) WITHOUT DOWNFLOWS.

R	$k_x = \frac{\sqrt{2}\pi}{r}, k_z = \frac{2\pi}{r}, \alpha = 90 \text{ cm s}^{-1}$							
	0°	5°	10°	15°	20°	25°	30°	35°
0.72	4.6(4)	4.3(4)	4.0(4)	3.6(4)	3.2(4)	2.6(4)	1.9(4)	4.4(3)
0.73	4.3(4)	4.0(4)	3.7(4)	3.4(4)	3.0(4)	2.5(4)	1.8(4)	4.1(3)
0.74	4.0(4)	3.8(4)	3.5(4)	3.2(4)	2.8(4)	2.3(4)	1.7(4)	3.7(3)
0.75	3.7(4)	3.5(4)	3.2(4)	2.9(4)	2.6(4)	2.1(4)	1.6(4)	3.3(3)
0.76	3.5(4)	3.3(4)	3.0(4)	2.7(4)	2.4(4)	2.0(4)	1.4(4)	3.4(3)
0.77	3.2(4)	3.0(4)	2.8(4)	2.5(4)	2.2(4)	1.8(4)	1.3(4)	3.1(3)
0.78	3.0(4)	2.8(4)	2.6(4)	2.3(4)	2.0(4)	1.7(4)	1.2(4)	2.8(3)
0.79	2.7(4)	2.5(4)	2.4(4)	2.1(4)	1.9(4)	1.6(4)	1.1(4)	2.6(3)
0.80	2.5(4)	2.3(4)	2.2(4)	2.0(4)	1.7(4)	1.4(4)	1.0(4)	2.4(3)
0.81	2.3(4)	2.1(4)	2.0(4)	1.8(4)	1.6(4)	1.3(4)	9.4(3)	2.2(3)
0.82	2.1(4)	1.9(4)	1.8(4)	1.6(4)	1.4(4)	1.2(4)	8.6(3)	2.0(3)
0.83	1.8(4)	1.7(4)	1.6(4)	1.5(4)	1.3(4)	1.1(4)	7.7(3)	1.8(3)
0.84	1.7(4)	1.5(4)	1.4(4)	1.3(4)	1.1(4)	9.5(3)	6.9(3)	1.6(3)
0.85	1.5(4)	1.4(4)	1.3(4)	1.2(4)	1.0(4)	8.4(3)	6.1(3)	1.4(3)
0.86	1.3(4)	1.2(4)	1.1(4)	1.0(4)	8.9(3)	7.4(3)	5.4(3)	1.2(3)
0.87	1.1(4)	1.1(4)	9.8(3)	8.9(3)	7.8(3)	6.5(3)	4.7(3)	1.1(3)
0.88	9.8(3)	9.1(3)	8.4(3)	7.6(3)	6.7(3)	5.6(3)	4.1(3)	9.3(2)
0.89	8.3(3)	7.8(3)	7.2(3)	6.5(3)	5.7(3)	4.8(3)	3.5(3)	7.9(2)
0.90	7.0(3)	6.5(3)	6.0(3)	5.4(3)	4.8(3)	4.0(3)	2.9(3)	6.6(2)
0.91	5.7(3)	5.3(3)	4.9(3)	4.5(3)	3.9(3)	3.3(3)	2.4(3)	5.5(2)
0.92	4.6(3)	4.3(3)	4.0(3)	3.6(3)	3.2(3)	2.6(3)	1.9(3)	4.4(2)
0.93	3.6(3)	3.3(3)	3.1(3)	2.8(3)	2.5(3)	2.0(3)	1.5(3)	3.4(2)
0.94	2.7(3)	2.5(3)	2.3(3)	2.1(3)	1.8(3)	1.5(3)	1.1(3)	2.5(2)
0.95	1.9(3)	1.7(3)	1.6(3)	1.5(3)	1.3(3)	1.1(3)	7.8(2)	1.8(2)
0.96	1.2(3)	1.1(3)	1.0(3)	9.4(2)	8.3(2)	6.9(2)	5.0(2)	1.1(2)
0.97	6.7(2)	6.2(2)	5.8(2)	5.2(2)	4.6(2)	3.8(2)	2.8(2)	6.4(1)
0.98	2.8(2)	2.6(2)	2.4(2)	2.2(2)	2.0(2)	1.6(2)	1.2(2)	2.7(1)
0.99	5.7(1)	5.3(1)	4.9(1)	4.5(1)	3.9(1)	3.3(1)	2.4(1)	5.5(0)
1.00	9.3(-2)	8.8(-2)	8.1(-2)	7.3(-2)	6.5(-2)	5.4(-2)	3.9(-2)	9.0(-3)

TABLE 4

TABLE 5
GROWTH TIME (YEAR) WITHOUT DOWNFLOWS.

R	$k_x = \frac{\sqrt{2}\pi}{r}$, $k_z = \frac{2\pi}{r}$, $\alpha = 90 \text{ cm s}^{-1}$								
	0°	5°	10°	15°	20°	25°	30°	35°	
0.72	4	4	4	5	6	7	10	46	
0.73	4	4	4	5	6	7	10	46	
0.74	4	4	4	5	6	7	10	48	
0.75	4	4	4	5	6	7	10	50	
0.76	4	4	4	5	6	7	10	46	
0.77	4	4	4	5	6	7	10	47	
0.78	4	4	4	5	6	7	10	47	
0.79	4	4	5	5	6	7	10	48	
0.80	4	4	5	5	6	7	10	48	
0.81	4	4	5	5	6	7	10	48	
0.82	4	4	5	5	6	7	11	49	
0.83	4	4	5	5	6	7	11	49	
0.84	4	4	5	5	6	8	11	49	
0.85	4	4	5	5	6	8	11	49	
0.86	4	4	5	6	6	8	11	49	
0.87	4	4	5	6	6	8	11	50	
0.88	4	4	5	6	6	8	11	50	
0.89	4	4	5	6	6	8	11	50	
0.90	4	4	5	6	6	8	11	50	
0.91	4	4	5	6	6	8	11	51	
0.92	4	4	5	6	6	8	11	51	
0.93	4	4	5	6	7	8	11	51	
0.94	4	5	5	6	7	8	11	51	
0.95	4	5	5	6	7	8	11	52	
0.96	4	5	5	6	7	8	11	52	
0.97	4	5	5	6	7	8	12	52	
0.98	4	5	5	6	7	8	12	53	
0.99	4	5	5	6	7	8	12	53	
1.00	4	5	5	6	7	9	12	54	

TABLE 6

RATIO OF POLOIDAL TO TOROIDAL FIELD (%) AS A FUNCTION OF RADIUS AND LATITUDE.

R	$k_x = \frac{\sqrt{2}\pi}{r}$, $k_z = \frac{2\pi}{r}$, $\alpha = 90 \text{ cm s}^{-1}$									$k_x = -\frac{\sqrt{2}\pi}{r}$, $k_z = -\frac{2\pi}{r}$, $\alpha = 5 \text{ cm s}^{-1}$								
	0°	5°	10°	15°	20°	25°	30°	35°	40°	45°	50°	55°	60°	65°	70°	75°	80°	85°
0.72	6	6	7	8	9	11	15	68	68	46	36	30	25	22	18	15	12	8
0.73	6	6	7	8	9	11	15	68	67	46	36	30	25	22	18	15	12	8
0.74	6	6	7	8	9	11	15	69	67	45	36	30	25	22	18	15	12	8
0.75	6	6	7	8	9	11	15	71	67	45	36	30	25	21	18	15	12	8
0.76	6	6	7	8	9	11	15	64	66	45	35	29	25	21	18	15	12	8
0.77	6	6	7	8	9	10	15	65	65	44	35	29	25	21	18	15	12	8
0.78	6	6	7	7	9	10	15	65	65	44	35	29	25	21	18	15	12	8
0.79	6	6	7	7	8	10	14	65	65	44	35	29	24	21	18	15	11	8
0.80	6	6	7	7	8	10	14	64	64	44	34	29	24	21	18	14	11	8
0.81	6	6	7	7	8	10	14	64	64	43	34	28	24	20	17	14	11	8
0.82	6	6	7	7	8	10	14	63	64	43	34	28	24	20	17	14	11	8
0.83	6	6	7	7	8	10	14	63	63	43	34	28	24	20	17	14	11	7
0.84	6	6	6	7	8	10	14	62	63	43	33	28	24	20	17	14	11	7
0.85	5	6	6	7	8	10	14	62	62	42	33	28	23	20	17	14	11	7
0.86	5	6	6	7	8	10	14	62	62	42	33	27	23	20	17	14	11	7
0.87	5	6	6	7	8	10	14	61	61	42	33	27	23	20	17	14	11	7
0.88	5	6	6	7	8	10	14	61	61	41	33	27	23	20	17	14	11	7
0.89	5	6	6	7	8	10	13	60	61	41	32	27	23	20	17	14	11	7
0.90	5	6	6	7	8	10	13	60	60	41	32	27	23	19	17	14	11	7
0.91	5	6	6	7	8	10	13	60	60	41	32	27	22	19	16	14	11	7
0.92	5	6	6	7	8	9	13	59	60	40	32	26	22	19	16	14	11	7
0.93	5	6	6	7	8	9	13	59	59	40	32	26	22	19	16	14	11	7
0.94	5	6	6	7	8	9	13	58	59	40	31	26	22	19	16	14	11	7
0.95	5	6	6	7	8	9	13	59	58	40	31	26	22	19	16	13	11	7
0.96	5	5	6	7	8	9	13	58	58	39	31	26	22	19	16	13	10	7
0.97	5	5	6	7	8	9	13	58	58	39	31	26	22	19	16	13	10	7
0.98	5	5	6	7	8	9	13	58	58	39	31	26	22	19	16	13	10	7
0.99	5	5	6	7	8	9	13	58	58	39	31	26	22	19	16	13	11	7
1.00	5	5	6	7	8	9	13	58	58	39	31	26	22	19	16	14	11	8